# A generic methodology for determination of drag coefficient of an aerostat envelope using CFD

Sagar M. Kale[*] , Pankaj Joshi[†] and  Rajkumar S. Pant[‡]
*Indian Institute of Technology Bombay, Mumbai, Maharashtra, 400 076, India*

**Aerostat envelopes are generally bodies of revolution with length to diameter ratio ranging from 3 to 5. Drag coefficient for this class of bodies can be obtained using empirical formulae or co-relations based on experimental studies. However such formulae are valid for specific class of envelope shapes only and result in errors of around 30% compared to the values determined by numerical methods. The motivation for the present study arose from the need for a simple but generic methodology to estimate coefficient of drag as a function of envelope geometry, thus eliminating the need for running numerically expensive CFD codes each time the shape is altered during an optimisation exercise. In a previous study, the envelop shape was parameterized in terms of six geometric coefficients, and a shape generation algorithm was developed to generate various possible shapes satisfying manufacturing and few geometric design constraints. An empirical co-relation for envelope drag coefficient was developed, but it was not amenable to coupling with an MDO process, since it required detailed geometric data about the envelope shape, especially the co-ordinates of several points at the nose and trailing edge, and the grid density in these regions. In the present study, around 600 feasible shapes satisfying the user-specified volume and length constraints were generated using the shape generation algorithm. The flow patterns over these shapes were studied using FLUENT[TM] CFD Package and a better co-relation was obtained by fitting a quadratic response surface using Design-Expert[TM] package. The current methodology uses only the values of six design variables to determine the drag coefficient, thus making it easy to integrate with a multi-disciplinary optimization algorithm for determining optimum envelope shape.**

## Nomenclature

| | | |
|---|---|---|
| $C_D$ | = | Coefficient of Drag |
| $C_{DV}$ | = | Envelope Drag coefficient using Volume$^{2/3}$ as reference |
| $C_{DS}$ | = | Envelope Drag Coefficient using envelope surface area as reference |
| $C_p$ | = | Pressure Coefficient |
| d | = | Envelope diameter, m |
| $F_{comp}$ | = | Composite Objective Function |
| L, $l$ | = | Length of aerostat envelope, m |
| S | = | Total surface area, m$^2$ |
| V | = | Envelope Volume, m$^3$ |
| $X_1$ | = | Abscissa of starting point of Spline -1 (m) |
| $X_2$ | = | Abscissa of starting point of Spline -2, Location of max. radius (m) |
| $X_3$ | = | Abscissa of end point of parabola (m) |
| $Y_1$ | = | Ordinate of the starting point of Spline -1 (m) |
| $Y_2$ | = | Ordinate of the starting point of Spline -2, Maximum radius (m) |
| $Y_3$ | = | Ordinate of the starting point of Parabola (m) |
| Re | = | Reynolds Number |
| g | = | Acceleration due to gravity, m/s$^2$ |

[*] Project Engineer, Aerospace Engineering Department, Powai, non-member AIAA
[†] Project Engineer, Aerospace Engineering Department, Powai, non-member AIAA
[‡] Associate Professor, Aerospace Engineering Department, Powai, Member AIAA

American Institute of Aeronautics and Astronautics

| | | |
|---|---|---|
| $\rho_a$ | = | Density of air, $m^3/kg$ |
| $\rho_{he}$ | = | Density of helium, $m^3/kg$ |
| $\sigma_{max}$ | = | Maximum hoop stress per unit thickness, N/m |
| RSM | = | Response Surface Methodology |

# I.    Introduction

An aerostat is an aerodynamically shaped body that is tethered to the ground. An Aerostat is filled with a 'lighter than air' gas, and thus generates static lift due to buoyancy. The primary requirements of an aerostat are high payload capacity, low blow-by, and sufficient stability and fast response to winds. The total lift that is produced by buoyancy and aerodynamic forces is balanced by the weight of the aerostat, the tether force and the payload. The buoyancy depends solely on the volume of LTA gas contained in the envelope. To increase the payload that can be carried by an envelope of fixed volume, either the weight of the aerostat has to be reduced or the tether force has to be reduced.

The weight of the envelope depends on its total surface area and the density of the material that is used for manufacturing the aerostat. Thus, to reduce the weight of the aerostat, its surface area should be reduced. Selection of the proper geometry of the hull can reduce the surface area of the hull for the same volume. However the surface area alone does not decide the shape of the envelope as there are other considerations such as stresses generated and drag produced in the aerostat. When stress is low, thinner fabrics with lesser density can be used for manufacturing the aerostat. Another method to reduce the weight of the envelope is to use patches of thicker and denser material in highly stressed regions and thinner materials for other regions.

Blow-by is the longitudinal displacement of the aerostat brought about by ambient winds. Such movement is undesirable, as it induces errors in the station keeping and reduces the effective operational altitude of the aerostat. If drag on the aerostat is high, longer tether has to be used to maintain the altitude, as shown in Fig. 1, thus drag also has a weight penalty attached to it.
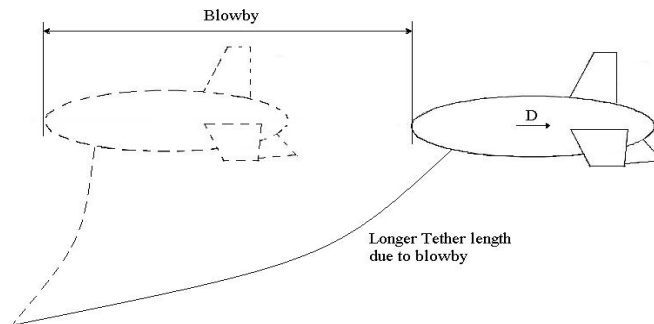


**Figure 1. Effect of blow-by on tether length**

To minimize blow-by, the lateral coefficient of drag of the aerostat should be kept to the minimum. The envelope drag constitutes nearly 67% of the total drag of the aerostat; hence selecting an appropriate envelope shape is very important.

**Drag minimization of axi-symmetric bodies**

In most cases, aerostat envelopes can be assumed to be axi-symmetric bodies of revolution. Many studies, both experimental[1-3], and computational[4-9] for obtaining low drag shapes of such bodies for various applications and Reynolds number regimes have been reported in literature. One of the most important considerations in interpreting the results of these studies is the characteristic length that is used to define the Reynolds number of the envelope. Though $V^{1/3}$ is usually used as the characteristic length, in some cases the Reynolds number reported is based on envelope length L. Transition Reynolds number depends on the choice of characteristic lengths. Similarly, the definition of coefficient of drag $C_D$ can also be based on total surface area of the body S, or the reference area equivalent to $V^{2/3}$.

The appropriate drag reduction technique to be followed requires knowledge of the working Reynolds number. Optimum shapes for different Reynolds number vary greatly. Maintaining extended regions of laminar flow by altering the shape of the body has been an important strategy in drag reduction for Envelope Reynolds number between $10^5$ and $10^8$. The shape of the body is selected to move the transition point as far back as possible. Although

theoretically an optimum shape can minimize the drag experienced by a body, proper manufacturing and smoothness of the shape is essential as the transition point shows a high sensitivity to surface roughness. Apart from passive laminarization techniques such as shape optimization, there are active methods of drag reduction such as boundary layer control.

## A. CFD techniques for shape optimization of axi-symmetric bodies

Parsons and Goodson[4] were the first to report application of numerical optimization techniques for shape optimization of axi-symmetric bodies. They represented the body by eight parameters, and coupled a boundary-layer method to a panel code. Pinebrook[8] has also carried out studies on drag minimization of bodies of revolution. Dodbele et al.[6] used the coordinate points defining the geometry of a fuselage as the design vector and the location of the transition point as the objective function to be maximized. The fact that drag reduction by modification of shape primarily involves increasing the extent of laminar flow justifies selection of location of transition point as objective function.

In contrast, Zedan et al.[5] used an inverse method for drag minimization of axi-symmetric bodies (such as airplane fuselages) by shaping. In this approach, a favorable velocity distribution was specified, and the shape of the body that produced this distribution was obtained. The fuselage designed showed a long region with a favorable pressure gradient in its forward part. It was stated that this should result in laminar flow up to 70 % of the body length at medium and large Reynolds numbers. Coiro and Nicolosi[7] have also reported some results related to Natural Laminar Flow on aircraft fuselages. In this method, a linearly varying doublet distribution is placed along the axis of the body such that the stagnation streamline gives the shape of the body. Starting with an initial guess shape, the strength of the singularities is varied until the velocity distribution over the shape matches the prescribed velocity distribution. This method is better than usual optimization methods as the physics of transition delay is not masked. It also involves less computational resources; however, it involves a lot of experience to decide the required velocity distribution.

Most of the abovementioned studies are related to bodies with extended laminar flow. However, Hess and James[9] have shown that in case of fully turbulent boundary layer, drag is insensitive towards changes in body contour, and significant drag reduction by shaping alone cannot be achieved in such cases. Bodies having fully turbulent flows show a flat drag minimum at $l/d$ ratios between 5 and 6.

Lutz and Wagner[10] have developed a tool for numerical optimization of axi-symmetric bodies submerged in incompressible flow at zero angle of attack. The objective of their work was to minimize the coefficient of drag of an envelope of given volume, for a prescribed speed range. In their studies, a panel code has been coupled with an integral boundary layer procedure to take into consideration the viscous effects. Instead of the conventional method of varying the shape of the body, the singularity strength distribution was varied during the optimization process and the optimum shape obtained from the stagnation streamline after closure conditions were satisfied. Transition calculations were done using a semi-empirical method known as the $e^n$ transition criterion. A hybrid optimizer was used, which enables constrained optimization and consists of Genetic Algorithms, Downhill simplex and a gradient method. The results of the study are shown in Fig. 2.
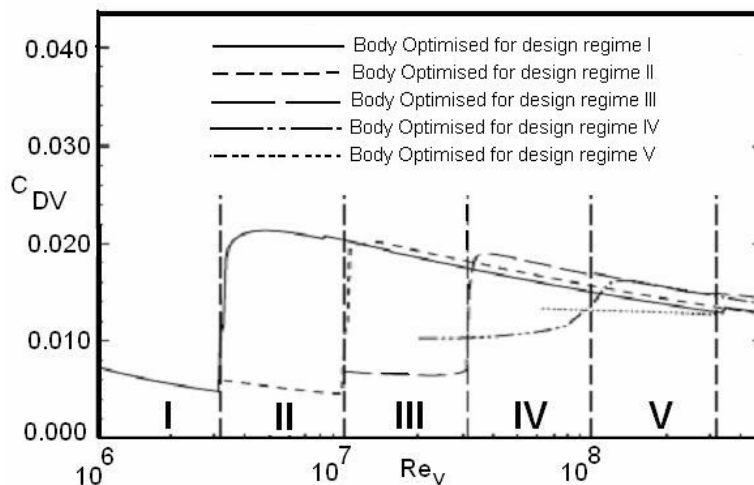


**Figure 2. $C_{Dv}$ for optimum shape for various Reynolds number regimes**[10]

$$\text{Design Regime I}: \mathrm{Re}_{V_I} = 1 \times 10^6 \ldots\ldots 3.16 \times 10^6 \quad (6 \le \mathrm{logRe}_{V_I} \le 6.5)$$

$$\text{Design Regime II}: \mathrm{Re}_{V_{II}} = 3.16 \times 10^6 \ldots\ldots 1 \times 10^7 \quad (6.5 \le \mathrm{logRe}_{V_{II}} \le 7)$$

$$\text{Design Regime III}: \mathrm{Re}_{V_{III}} = 1 \times 10^7 \ldots\ldots 3.16 \times 10^7 \quad (7 \le \mathrm{logRe}_{V_{III}} \le 7.5) \tag{1}$$

$$\text{Design Regime IV}: \mathrm{Re}_{I_V} = 3.16 \times 10^7 \ldots\ldots 1 \times 10^8 \quad (7.5 \le \mathrm{logRe}_{I_V} \le 8)$$

As the design Reynolds number increases, the favorable pressure gradient in the fore body region has to be increased, in order to delay transition. This can be done by increasing the diameter, or moving the point of maximum diameter forward. The maximum diameter is fixed by the pressure recovery that is possible without turbulent separation. In real life airship and aerostat applications, the maximum diameter is also governed by the stresses that are developed in the fabric. However this factor wasn't taken into consideration by Lutz and Wagner[10] and the aerodynamic aspects were alone taken into account for optimization. Transition occurs close to the point of minimum pressure. Beyond the point of transition, the wetted surface should be reduced as much as possible to minimize skin friction drag.

**Shape optimization by variation of geometric parameters**
 Several low-drag profiles suitable for airship and aerostat envelopes have been suggested in literature. The approach is primarily to develop shapes that delay transition and separation. One of the frequently used methods of shape optimization is expressing the body profile as a combination of simple geometric shapes. Once the geometry of the body has been established in terms of simple curves, the defining parameters of these curves can be used as design variables. The shape defined by the optimum combination of these parameters is the shape for minimum drag.
 Two such shapes are the NPL shape[11] suggested by National Physics Laboratory and the GNVR shape[12,13] developed by National Aerospace Laboratories, India. The NPL shape consists of two ellipsoids of revolution, which meet at the location of maximum diameter, as shown in Fig.3. The major axis of the rear ellipsoid is √2 times the major axis of the front ellipsoid. The radius of curvature continuously increases thus reducing the possibility of flow separation.



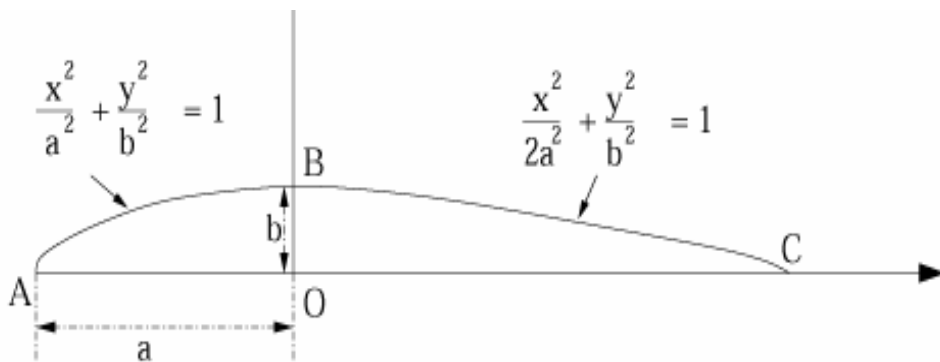**Figure 3. NPL shape**

The GNVR shape is a combination of an ellipse, circle and parabola as shown in Fig. 4. Earlier computational[12] and experimental studies[13] have indicated that this shape corresponds to low $C_D$ of aerostats operating at $M = 0.1$ and $H = 1.0$ km. The entire geometry of GNVR is parameterized in terms of its maximum diameter, as shown in Fig. 4.

American Institute of Aeronautics and Astronautics
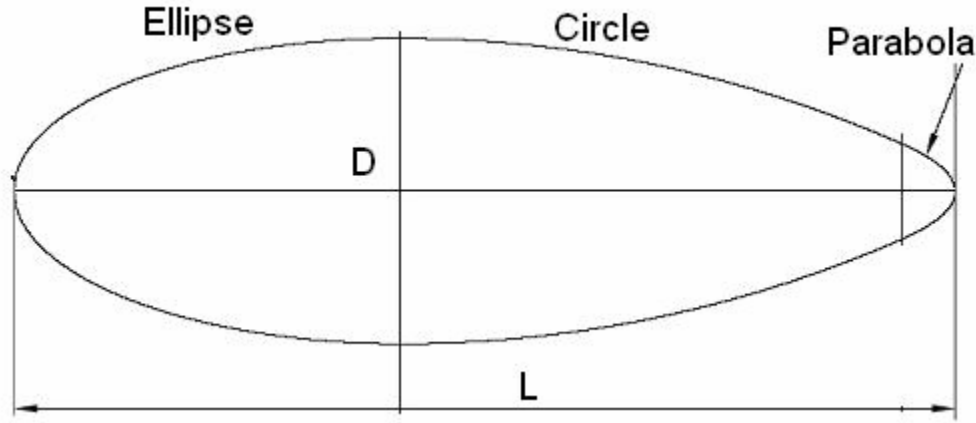
$$\text{Nose Ellipse} - \text{Origin to } 1.25D \quad : \frac{X^2}{1.25\,D^2} + \frac{Y^2}{0.5\,D^2} = 1$$

$$\text{Middle Circle} - 1.25\,D \text{ to } 1.62D: \ X^2 + (Y - 3.5\,D)^2 = 16\,D^2$$

$$\text{Tail Parabola} - 1.62\,D \text{ to } 1.8D \quad : Y^2 = 1.373\,D(1.8\,D - X)$$

**Figure 4. GNVR envelope profile**

## II.  Multidisciplinary approach to envelope shape optimization

Kanikdale et al.[14] have attempted a multidisciplinary approach to shape optimization of airships envelopes. They have defined a generic envelope profile in terms of a combination of two cubic-splines, with a spherical cap in the front portion, and a parabolic shape in the end, as shown in Fig. 5. The selection of a spherical cap for the enables the shape to be compatible with the spherical mooring cups that are in use in the winching and mooring systems of aerostats. A parabola was selected for the rear portion to make attachment of fins easier.
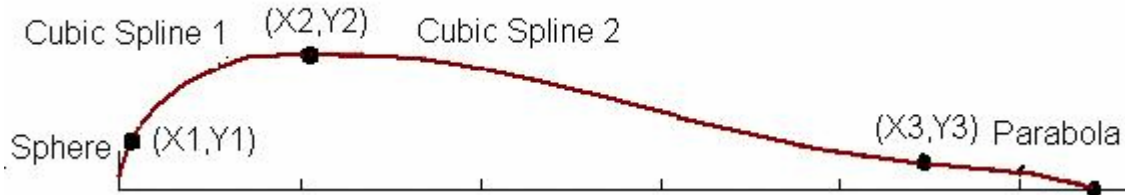


**Figure 5. Parameterization of envelope geometry by Kanikdale et al[12].**

The defining equations in Kanikdale et al's[14] formulations are:

| | | |
|---|---|---|
| Spherical Cap: | $y^2 = 2xR - x^2$ | |
| Spline I: | $y = a_1 x^3 + b_1 x^2 + c_1 x + d_1$ | (2) |
| Spline II: | $y = a_2 x^3 + b_2 x^2 + c_2 x + d_2$ | |
| Parabolic end: | $y^2 = a_n(L - x)$ | |

There are 11 parameters in this formulation viz., $R$, $a_1$, $b_1$, $c_1$, $d_1$, $a_2$, $b_2$, $c_2$, $d_2$, $a_n$ and $L$, For an envelope of given volume, five of these can be eliminated using the continuity of slope at the junction of various curves, and the fact that the junction of two splines represents the point of maximum diameter. Thus the shape can be expressed as a function of the following six shape parameters:

$$XD = (x1, \ x2, \ y2, \ x3, \ y3, \ l) \tag{3}$$

An algorithm was developed that generated the co-ordinates of a feasible shape for specified values of the above six shape parameters, which were varied within a specified the range. Certain combinations of the abovementioned design variables could lead to "wiggly" envelope shapes. Such shapes were filtered out by forcing a constraint on

5

negative radius of curvature, since the shapes with convex curvature (particularly at the trailing portion) would suffer from heavy pressure drag. Shapes with rate of change of curvature beyond a specified value were also filtered out, since they would lead to a greater penalty in terms of manufacturing.

The shape was optimized to minimize the envelope drag, the stresses developed in the envelope fabric and the weight of the envelope. A composite objective function involving $C_{DV}$, $\sigma_{max}$ and S of the envelope was formed as:

$$F_{comp} = w_1 \left[ \frac{C_{DV}}{(C_{DV})_{GNVR}} \right] + w_2 \left[ \frac{S}{(S)_{GNVR}} \right] + w_3 \left[ \frac{\sigma_{max}}{(\sigma_{max})_{GNVR}} \right] \tag{4}$$

Where, $w_1$, $w_2$ and $w_3$ are weight functions. The GNVR shape was taken as reference shape for comparison. Optimum shapes for minimum value of various objective functions were obtained by coupling SIMANN Simulated Annealing optimizer. The resulting optimum shape compared with the GNVR shape is shown in Fig.6, and the comparison of values for the three objective functions with the GNVR shape is listed in Table 1.
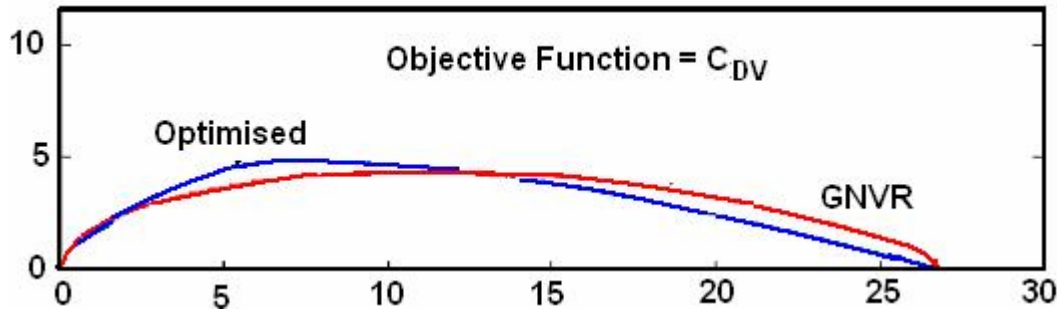


**Figure 6. Comparison of GNVR shape and Optimized shape**

**Table 1 Comparison of values for the three objective functions with GNVR shape**

| Objective Function | GNVR Shape | Optimized Shape | % Improvement |
|---|---|---|---|
| $C_{DV}$ | 2.686E-02 | 2.260 E-02 | 15.8 % Lower |
| S | 573 | 598 | 4.5 % Higher |
| $\sigma_{max}$ | 4457 | 4262 | 4.4 % Lower |
| $F_{comp}$ | 3.0 | 2.8 | 6.7 % Lower |

## B. Formulation of an expression for $C_{DV}$ in terms of envelope geometrical parameters

An empirical formula for $C_{DV}$ has been suggested by Hoerner[11],

$$C_{DV} = \frac{0.172\,(l/d)^{1/3} + 0.252\,(l/d)^{0.833} + 1.032\,(l/d)^{0.3704}}{Re^{1/6}} \tag{5}$$

Equation (5) is based on experimental studies, and hence valid only for specific class of envelope shapes with limits on range of $l/d$ and position of maximum diameter. Kanikdale et al.[12] estimated $C_{DV}$ using Eqn. 2 for several axi-symmetric bodies of revolution, and found that it resulted in errors of around 30% compared to the values determined by the FLUENT[TM] CFD Package.

Based on a detailed study of results obtained through CFD experimentation over a large number of shapes, Kanikdale et. al. developed an empirical procedure for estimation of $C_{DV}$, which is listed vide Eqs. (6-9)

$$C_{DV} = A\alpha + B \tag{6}$$

American Institute of Aeronautics and Astronautics

Where,

$$\alpha = \alpha_1 . \alpha_2^\beta . \alpha_3 . X_{y\,max} \tag{7}$$

and

$$\beta = \frac{214}{(l/d)} - 31.26; \text{ for } \beta > 3$$
$$= 3 \quad \text{otherwise} \tag{8}$$

The values for the parameters $\alpha_1$, $\alpha_2$ and $\alpha_3$ were specified as:

$$\alpha_1 = \frac{d}{l - X_{y\,max}}; \alpha_2 = \sum_{x=0.9l}^{l} \frac{dy/dx}{l.N}; \ \alpha_3 = \sum_{x=0}^{0.1l} \frac{dy/dx}{l.N} \tag{9}$$

Where N = Number of Grid Points used in the CFD analysis

## C. Limitations of Kanikdale's empirical formula for $C_{DV}$ Estimation

Kanikdale et al's model[14] for $C_{DV}$ estimation is not amenable for coupling with an MDO process, since it requires the knowledge of the slope of nose and tail portion, for which it requires detailed geometric data about the envelope shape, especially the co-ordinates of several points at the nose and trailing edge, and the grid density in these regions. Secondly, the selection of the parameters (such as $\alpha_1$, $\alpha_2$, $\alpha_3$, $\beta$) for fitting an expression for $C_{DV}$ is quite arbitrary, and do not reflect the physics of the flow.

## D. Modified Approach for obtaining a co-relation for Drag Coefficient

The present work attempts to arrive at a more generic methodology to calculate the envelope drag coefficient of an aerostat of given volume and length. The current methodology uses only the values of six shape parameters to determine the drag coefficient, making it easy to integrate with an MDO process.

The envelope geometry was parameterized using the same six shape parameters as in the previous study by Kanikdale et al[14]. The dimensions of an envelope of GNVR shape for an envelope volume of 2000 m³ were obtained, and these were used to decide the ranges for the six shape parameters, as shown in Table 2.

**Table 2 Upper and Lower limits imposed on the shape parameters**

| Shape Parameters | Lower Limit (m) | Upper Limit (m) |
|---|---|---|
| $X_1$ | 0.05 | 2.00 |
| $Y_2$ | 0.5 | 5.00 |
| $X_2$ | 0.5 | 18.0 |
| $X_3$ | 0.6 | 36.0 |
| $Y_3$ | 0.5 | 4.5 |
| L | 35.0 | 36.0 |

With the help of shape generation algorithm, around 600 feasible shapes were generated, and their $C_{DS}$ values were obtained using the FLUENT$^{TM}$ CFD code. An axi-symmetric grid was built around the upper half of the body in the semicircular computational domain, and an axi-symmetric segregated implicit solver was selected, in conjunction with S-A turbulence model. The required boundary condition parameters i.e., pressure, temperature and density were obtained using ISA conditions corresponding to altitude of 1.2 Km. Sutherland's formula was selected for viscosity variation with temperature. The pressure distribution and $C_{DS}$ were obtained for a Gauge Pressure of 87514 Pa, and Mach No. of 0.107.

The flow patterns generated over the various shapes were studied to correlate them with the geometric features of the aerostat envelope. Figure 7 shows the effect of variation of each shape parameter individually on the values of $C_{DS}$.
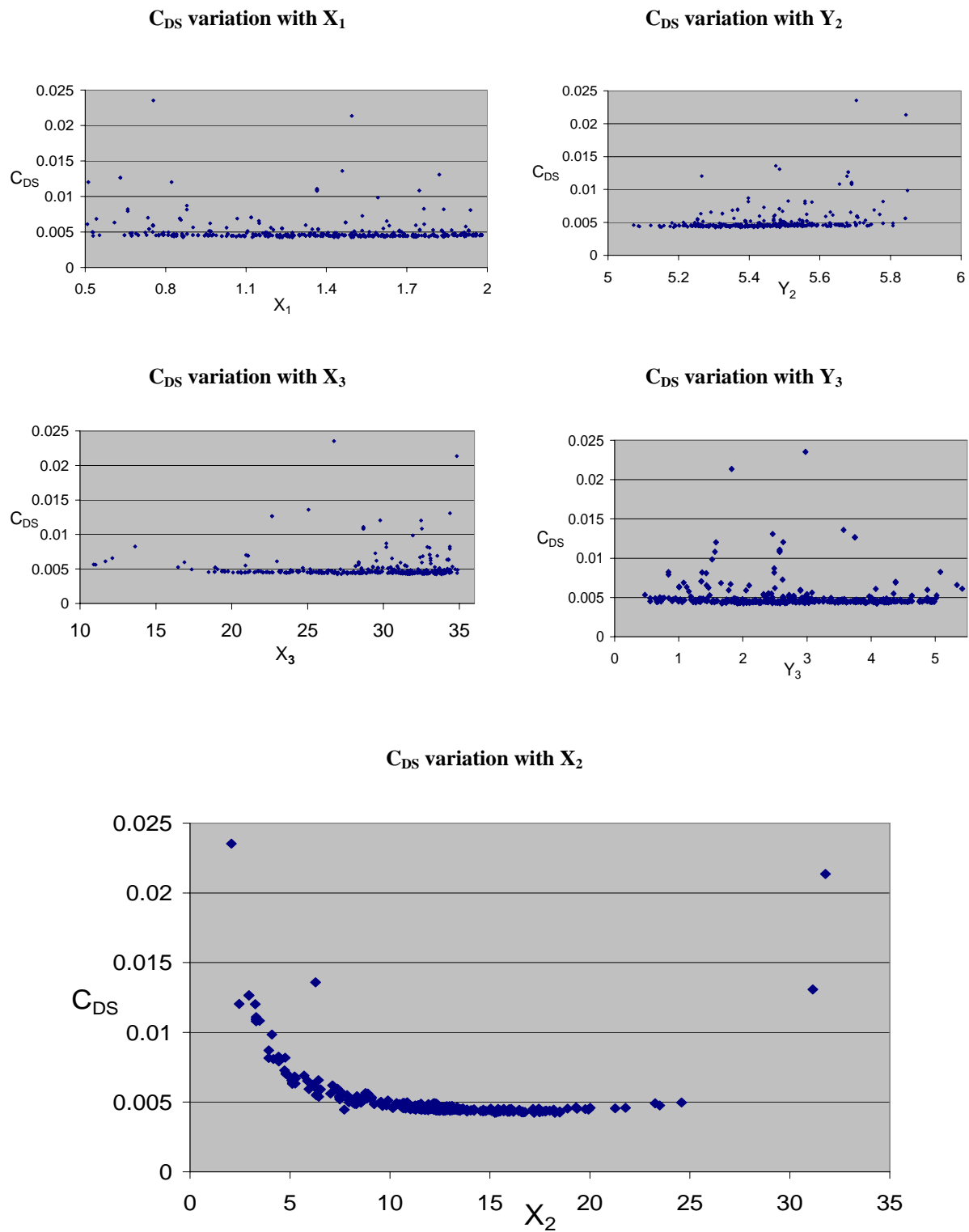
American Institute of Aeronautics and Astronautics

**$C_{DS}$ variation with $X_1$**

**$C_{DS}$ variation with $Y_2$**

**$C_{DS}$ variation with $X_3$**

**$C_{DS}$ variation with $Y_3$**

**$C_{DS}$ variation with $X_2$**

**Figure 7. Effect of variation of each shape parameter individually on $C_{DS}$**

American Institute of Aeronautics and Astronautics

It was observed that $C_{DS}$ increased exponentially with reduction in $X_2$ values less than around 10.0 m, i.e., bodies with their maximum diameter located within the first 30% of the length had high $C_{DS}$. No clear-cut trend for $C_{DS}$ was seen with the variation of the other five shape parameters, indicating that their effect on $C_{DS}$ is only of a lower order.

A closer look at the flow patterns and the variation of $C_{DS}$ with $X_2$, revealed that the shapes could be classified into three distinct regimes; those having $X_2$ upto 25% of length (Regime-I), those for which $X_2$ between 25% and 50% (Regime-II), and those for which $X_2$ was more than 50% of the length (Regime-III), as shown in Fig.8.
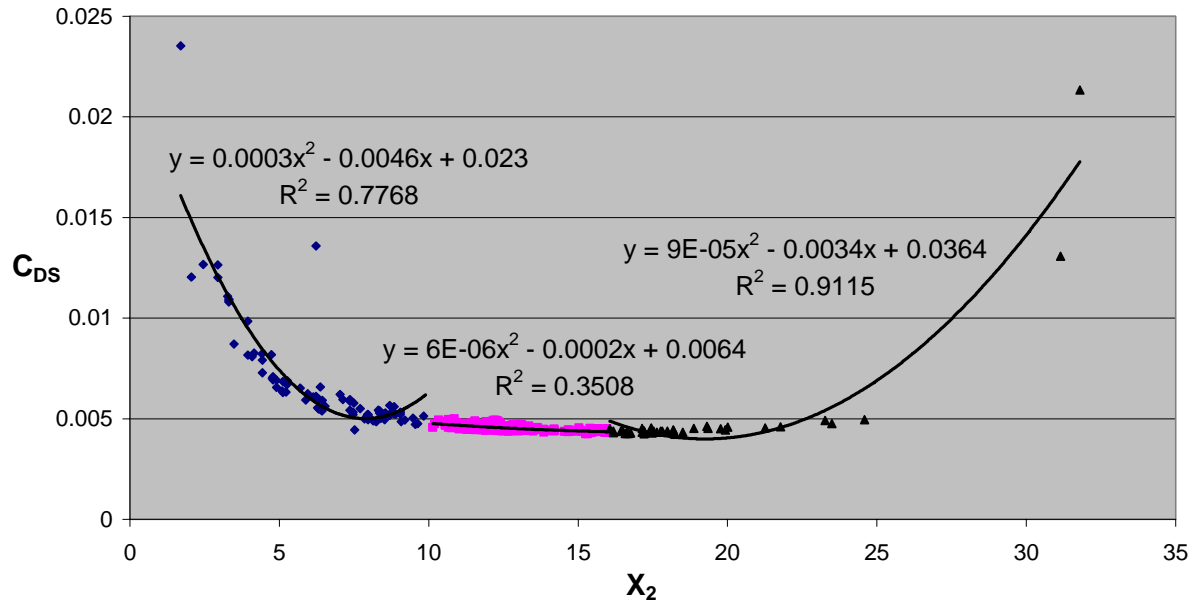
## Variation of $C_{DS}$ With $X_2$



$$y = 0.0003x^2 - 0.0046x + 0.023$$
$$R^2 = 0.7768$$

$$y = 9E\text{-}05x^2 - 0.0034x + 0.0364$$
$$R^2 = 0.9115$$

$$y = 6E\text{-}06x^2 - 0.0002x + 0.0064$$
$$R^2 = 0.3508$$

**Figure 8. The three regimes based on variation of $C_{DS}$ with $X_2$**

Sample flow patterns and $C_p$ distribution along envelope length for one representative shape belonging to each of these regimes is shown in Fig. 9
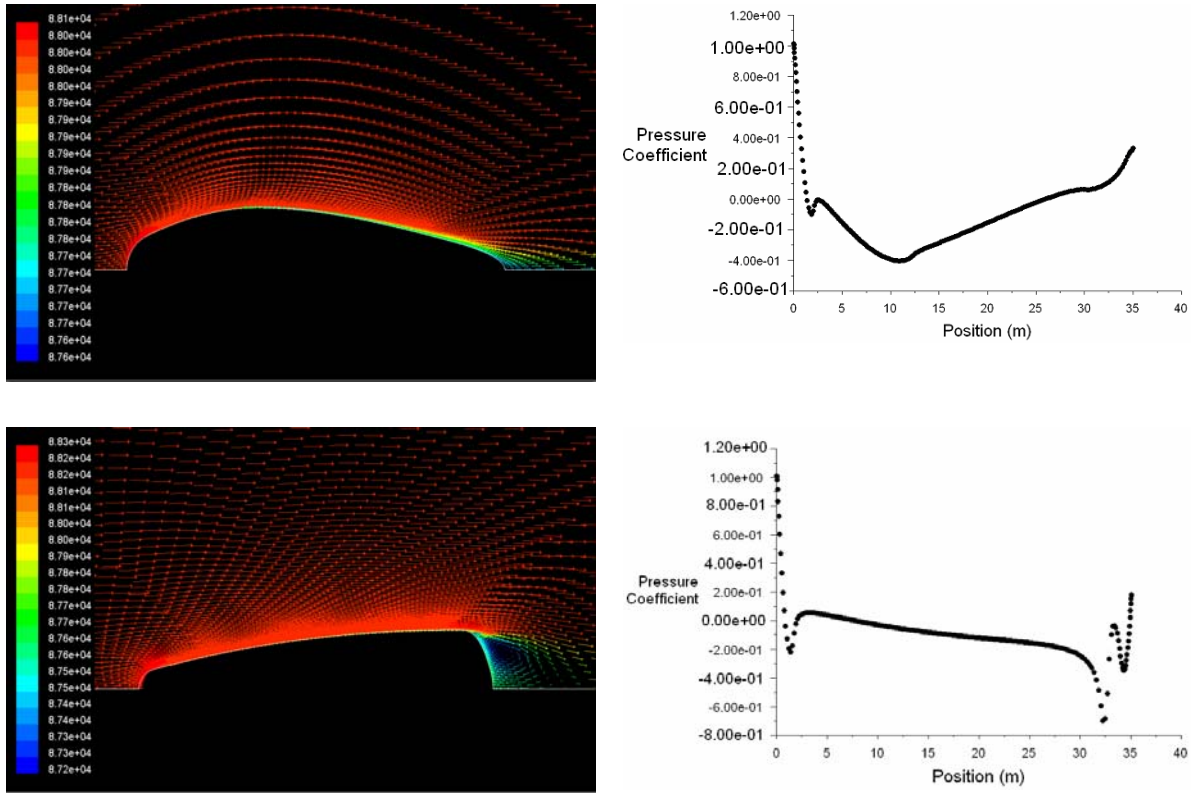


9
American Institute of Aeronautics and Astronautics
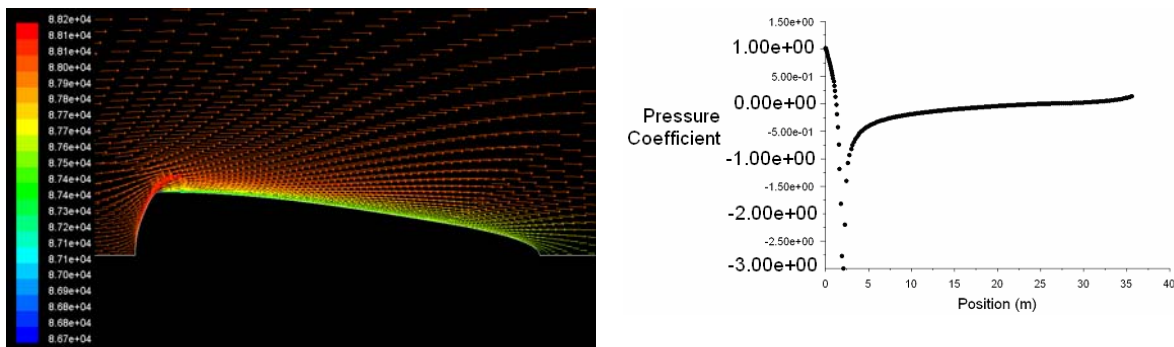
**Figure 9. Typical flow patterns and $C_p$ distribution along envelope length in three regimes**

### E. Response Surface methodology for better co-relation

Response Surface Methodology, or RSM, is a collection of mathematical and statistical techniques that are useful for the modeling and analysis of problems in which a response of interest is influenced by several variables and the objective is to optimize this response. The approach of RSM is to perform a series of experiments, based on numerical analyses or physical experiments, for a prescribed set of design points, and to construct a global approximation of the measured quantity over the design space, as shown in Fig. 10. RSM has been gainfully employed for diverse applications, ranging from aerodynamics and rocket propulsion[15] to drug dosage design[16].
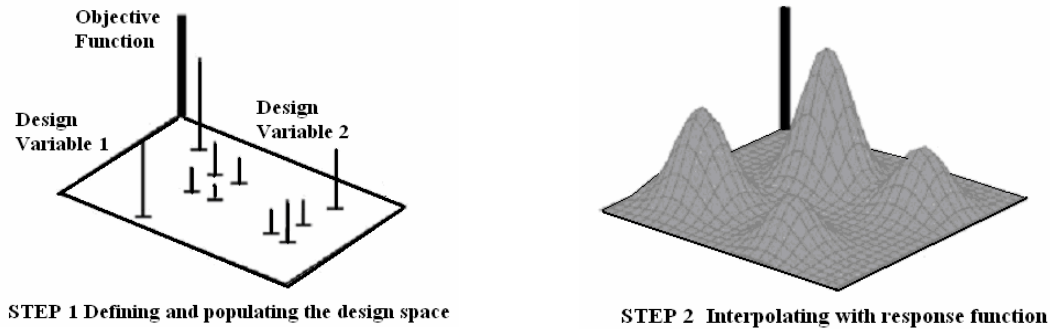


STEP 1 Defining and populating the design space     STEP 2 Interpolating with response function

**Figure 10. Basic methodology adopted in Response Surface Method[15]**

According to Myers and Montgomery[17], RSM tends to reduce the number of computational or physical experiment necessary to explore the design space. Another advantage of using response surface analysis is the ability to intelligently choose only a few of the full factorial set to construct an input-output relationship.

A second-order response surface was developed in the present study, for obtaining the co-relations between $C_{DS}$ and the shape parameters. This is because a first order polynomial would not have incorporated the various interaction terms of shape parameters, and higher order polynomial other than quadratic would have resulted in

lower goodness of fit and reliability over the entire parameter space. The Central Composite Design (CCD) scheme was selected for the design of the response surface design, since it is considered to be the most reliable class for fitting a second-order response surface.

Box and Hunter[18] suggested that a second-order response surface design should be rotatable, to provide good predictions throughout the region of interest. In a rotatable design, the variance of the predicted response is the same at all points that are the same distance from the design center. The selection of a parameter "Alpha," in coded units, is the axial distance from the center point and makes the design rotatable. A rotatable design provides equally good predictions at points equally distant from the center, a very desirable property for RSM.

The response surface was developed using the CCD module in *Design Expert*[19], incorporating all quadratic terms and their interactions. These terms were then analyzed on the basis of ANOVA tests, and the insignificant terms were neglected to develop an improved response surface. This iterative process was repeated, till adequate response surface fits were achieved; the resultant quadratic response surface is listed in Eqs. (10-12).

For Regime-I
$$C_{DS} = \alpha_1 + \alpha_2 X_2 + \alpha_3 Y_2 + \alpha_4 X_2{}^2 + \alpha_5 X_2 Y_2 \tag{10}$$

For Regime-II
$$C_{DS} = \beta_1 + \beta_2 X_2 + \beta_3 X_3 + \beta_4 Y_2 + \beta_5 Y_3 + \beta_6 X_2{}^2 + \beta_7 X_2 Y_2 \\ + \beta_8 X_3 Y_2 + \beta_9 X_3 Y_3 + \beta_{10} Y_2 Y_3 \tag{11}$$

For Regime-III
$$C_{DS} = \lambda_1 - \lambda_2 X_1 - \lambda_3 X_2 - \lambda_4 Y_2 - \lambda_5 Y_3 - \lambda_6 L + \lambda_7 X_1{}^2 \\ + \lambda_8 X_2{}^2 + \lambda_9 Y_2{}^2 + \lambda_{10} Y_3{}^2 + \lambda_{11} X_1 X_2 - \lambda_{12} X_1 Y_3 + \lambda_{13} Y_2 L \tag{12}$$

The values of the coefficients $\lambda_1, \lambda_2 \dots \lambda_{13}$ in Eqs. (10-12) are listed in Appendix.

The results of ANOVA test for the final model is shown in Table 3. High values of $R^2$, Adjusted $R^2$ and Predicted $R^2$ indicate that the response surface developed for different regimes match well with the experimental data. Another indication of the goodness of the fit is the close agreement between the values of $R^2$, Adjusted $R^2$. Further, the values of Predicted $R^2$ and Adjusted $R^2$ values are also within 0.20 of each other, which indicates low variability in predicting any new value.

**Table-3 Results of ANOVA test**

|  | Regime-I | Regime-II | Regime-III |
|---|---|---|---|
| $X_2$ location | $X_2 < 0.25L$ | $0.25L \leq X_2 < 0.5\,L$ | $X_2 \geq 0.50L$ |
| $R^2$ | 0.9887 | 0.9514 | 0.9445 |
| Adjusted $R^2$ | 0.9854 | 0.9498 | 0.9334 |
| Predicted $R^2$ | 0.9805 | 0.9455 | 0.9035 |

A plot of actual and predicted values of $C_{DV}$ for the three regimes is shown in Fig.11, which show a good match along the entire range. The scatter in the predicted values of $C_{DS}$ is shown in Fig.12. No specific trend in the scatter of predicted values is seen, indicating that no important co-relation terms (that would have greatly altered the equations for the response surface) have been left out. Another test on the goodness of the response surface are the normal probability plots, which indicate whether the residuals follow a normal distribution, in which case the points follow a straight line and show that results are consistent with normality. These plots for various regimes are shown Fig.13.

All the above statistical tests and plots provide confidence toward the good quality and high reliability of the response surface obtained.
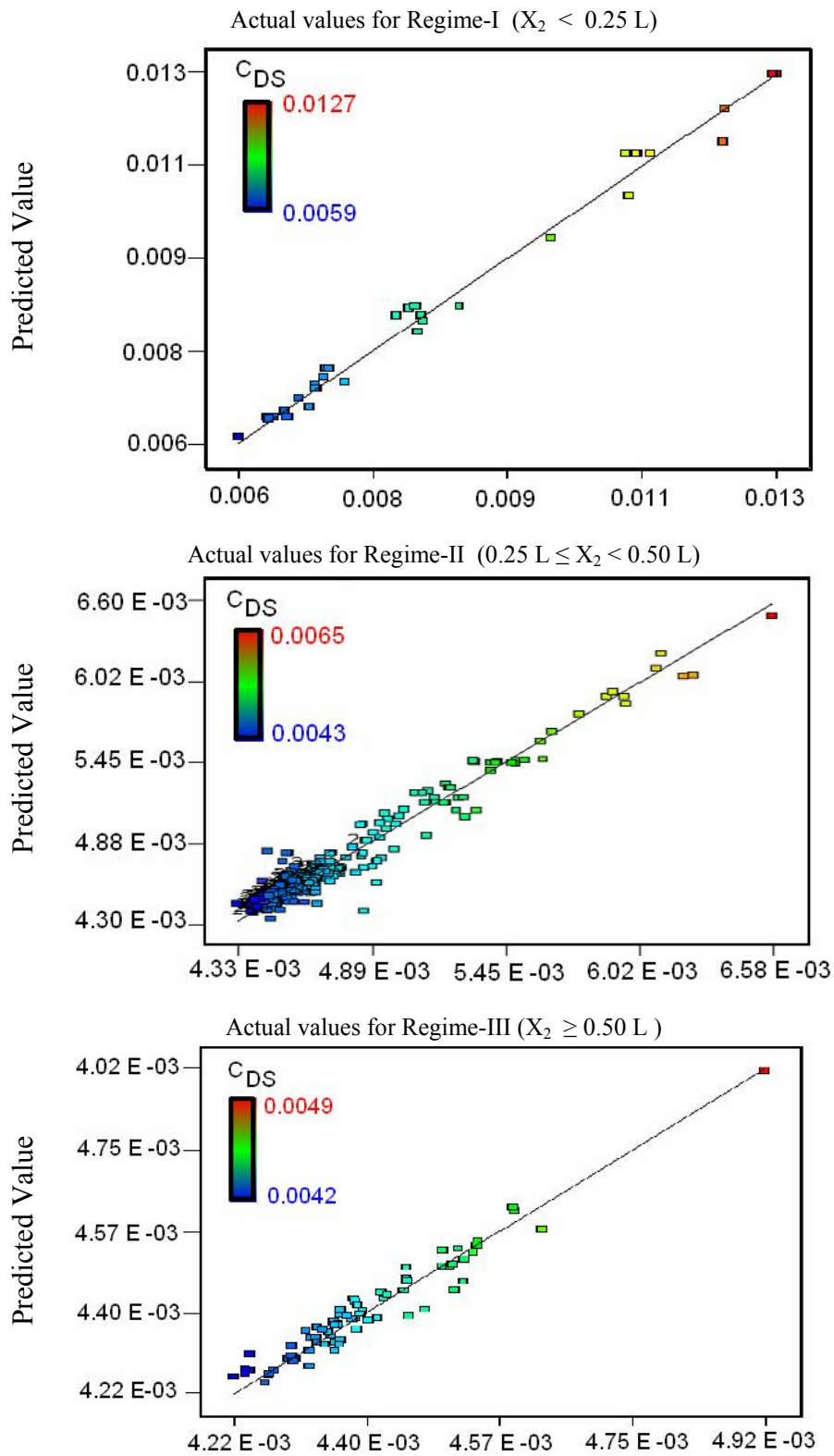
Actual values for Regime-I ($X_2 < 0.25$ L)



Actual values for Regime-II ($0.25$ L $\leq X_2 < 0.50$ L)



Actual values for Regime-III ($X_2 \geq 0.50$ L )



**Figure 11. Predicted v/s Actual value of CD$_S$ for the points in three regimes**

American Institute of Aeronautics and Astronautics

Predicted values for Regime-I ($X_2 < 0.25$ L)

Predicted values for Regime-II ($0.25$ L $\leq X_2 < 0.50$ L)

Predicted values for Regime-III Regime-III ($X_2 \geq 0.50$ L )
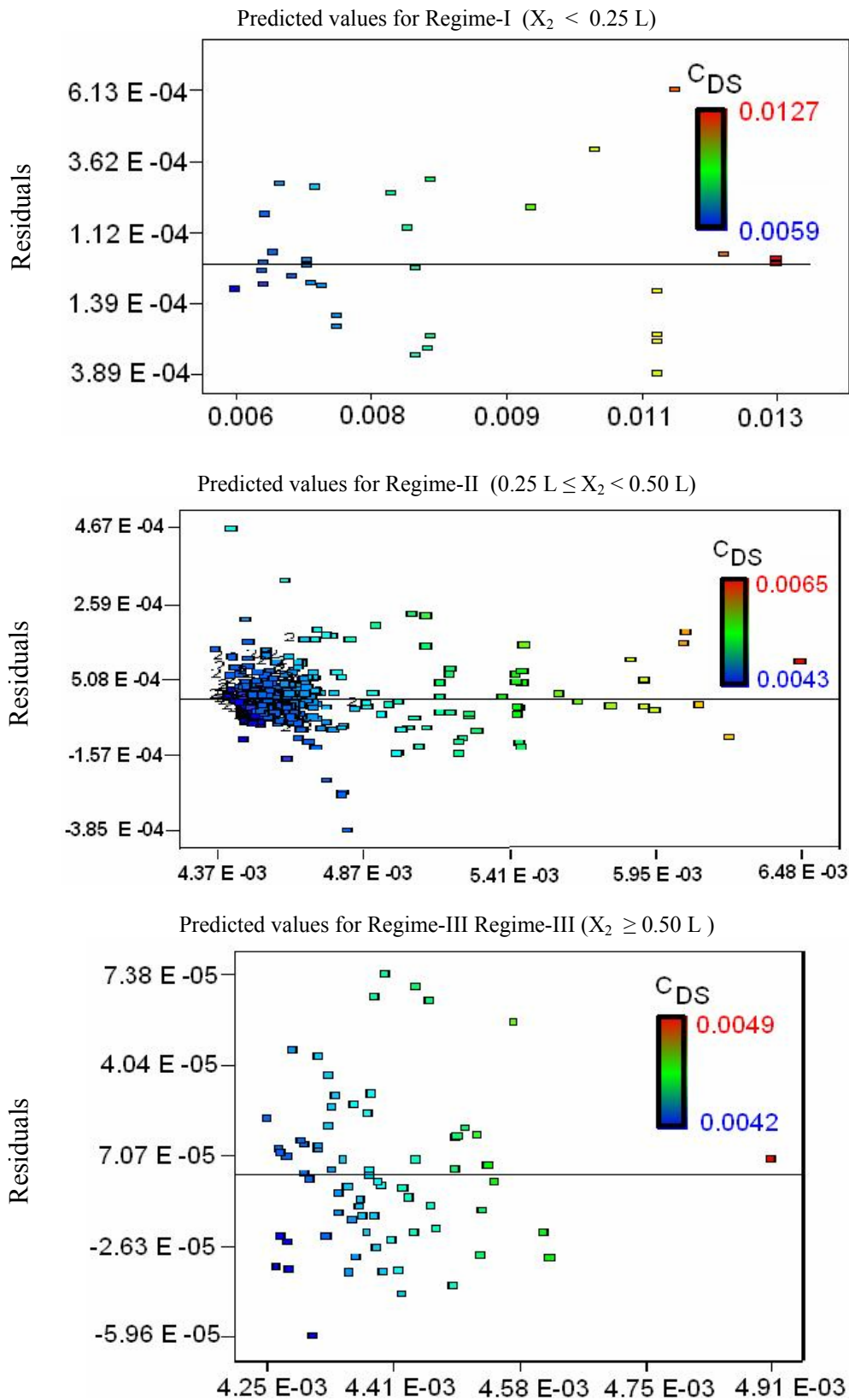
**Figure 12. Residuals of the Predicted value of $C_{DS}$ for the points in three regimes**

American Institute of Aeronautics and Astronautics
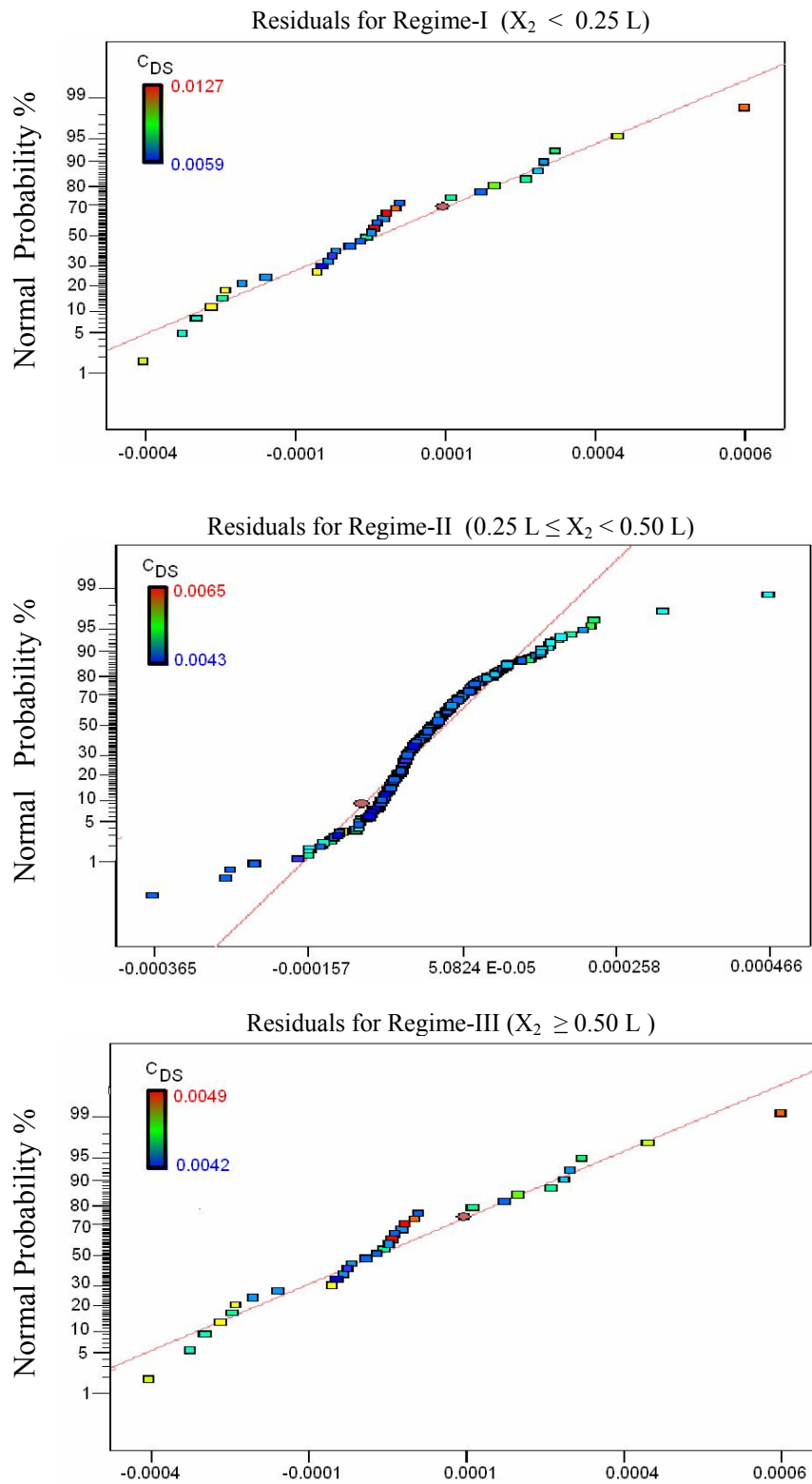
**Figure 13. Normal Probability Vs Residuals for the points in three regimes**

American Institute of Aeronautics and Astronautics

### III.     Conclusions

In the present work, an improved co-relation for drag coefficient of a generic axi-symmetric body of revolution has been developed. The shape of the body was parameterized with six shape parameters, using Kanikdale's shape generation algorithm. A strong co-relation between drag coefficient and one shape parameter (viz., location of the point of maximum thickness) was observed, with other parameters not contributing much. A second-order response surface, including several interactive quadratic terms was fitted to incorporate the effect of all shape parameters, which can estimate $C_{DS}$ with an accuracy of $\pm 10$ %, compared to the results obtained with FLUENT$^{TM}$ CFD code. Based on the results of the various statistical parameters and test, it was concluded that the response-surface obtained is accurate and reliable.  This response surface can be coupled with a high level of confidence to multi-disciplinary analysis and optimization procedure, without the need for calling a CFD routine for estimation of the Drag Coefficient.

### Appendix

The values of the coefficients for the response surface obtained for the three segments are listed below.

| Coefficients | Value | Coefficients | Value |
|---|---|---|---|
| $\alpha_1$ | -1.89E-02 | $\beta_{10}$ | −2.80E -04 |
| $\alpha_2$ | 2.40E-04 | $\lambda_1$ | 9.79E -02 |
| $\alpha_3$ | 8.00E-03 | $\lambda_2$ | -7.10E -04 |
| $\alpha_4$ | 4.80E-04 | $\lambda_3$ | -3.50E -04 |
| $\alpha_5$ | 1.10E-03 | $\lambda_4$ | -2.30E -02 |
| $\beta_1$ | -1.56E-02 | $\lambda_5$ | -5.77E -04 |
| $\beta_2$ | 5.30E-04 | $\lambda_6$ | -1.46E -03 |
| $\beta_3$ | 2.20E-04 | $\lambda_7$ | 1.00E -04 |
| $\beta_4$ | 5.62E-03 | $\lambda_8$ | 9.00E -06 |
| $\beta_5$ | 5.80E-04 | $\lambda_9$ | 1.35E -03 |
| $\beta_6$ | 2.40E-05 | $\lambda_{10}$ | 1.50E -05 |
| $\beta_7$ | -2.20E-04 | $\lambda_{11}$ | 3.50E -05 |
| $\beta_8$ | -7.20E-05 | $\lambda_{12}$ | -2.20E -05 |
| $\beta_9$ | 2.00E-05 | $\lambda_{13}$ | 2.43E -04 |

### Acknowledgements

### References

[1]Gertler, M., "Resistance Experiments on a Systematic Series of Streamlined Bodies of Revolution - for Application to the Design of High Speed Submarines," *Navy Department, Report C-297*, Central Air Documents Office, Wright Patterson Air Force Base, Dayton, Ohio, April 1950.

[2]Carmichael, B.H., "Underwater Drag Reduction through Optimum Shape*,"* AIAA *Second Propulsion Joint Specialist Conference*, Colorado Springs, Colorado, June 13–17, 1966.

[3]Hansen R. J., and Hoyt J. G., "Laminar-To-Turbulent Transition on a Body of Revolution with an Extended Favorable Pressure Gradient Fore body", *Journal of Fluids Engineering*, Vol. 106, June 1984, pp. 202–210.

[4]Parsons, J. S., and Goodson, R.H. "Shaping of Axisymmetric Bodies for Minimum Drag in Incompressible Flow," *Journal of Hydronautics*, Vol. 8, No. 3, 1974.

[5]Zedan, M. F., Seif, A. A., and Al-Moufadi S., "Drag Reduction of Airplane Fuselages through Shaping by the Inverse Method", *Journal of Aircraft*, Vol. 31, No. 2, March-April 1994.

[6]Dodbele, S. S., van Dam C. P., Vijgen, P. M. H. W, and Holmes, B. J., "Shaping of Airplane Fuselages for Minimum Drag,"*AIAA Paper* 86-0316 1986.

[7]Coiro, D. P., and Nicolosi, F., "Design of Natural Laminar Flow Fuselages," 19th International Council of the Aeronautical Sciences Congress Anaheim California, USA Sept. 1994.

[8]Pinebrook, W. E., "Drag Minimization on a Body of Revolution,"Dissertation at the Faculty of the Department of Mechanical Engineering, University of Houston, 1982.

[9]Hess, J.L., and. James, R. M., "On the Problem of Shaping an Axisymmetric body to obtain Low Drag at Large Reynolds Numbers," Douglas Aircraft Company, Long Beach, CA, Report MDC J6791, January 1975.

[10]Lutz, T., and Wagner, S., "Drag Reduction and Shape Optimization of Airship bodies," *Journal of Aircraft*, Vol. 35, No. 3, May- June 1998, pp 345-351.

[11]Khoury, G. A., Gillett, J. D., Eds., *Airship Technology*, Cambridge Aerospace Series: 10, ISBN 0-521-430-747, Cambridge University Press, Cambridge 1999.

[12]Narayana C. L., and Srilatha, K. R., Analysis of aerostat configurations by panel methods, *BLISS Project Document CF 0010*, National Aerospace Laboratories, Bangalore, India, July 2000.

[13]Sundaram, S, Wind Tunnel tests on 1:7 and 1:28 scale Aerostat Models Experimental Aerodynamics Divisions, National Aerospace Laboratories, Bangalore, India, February 2000.

[14]T. Kanikdale, A. Marathe and R. Pant, Multi-Disciplinary Optimization of Airship Envelope Shape, Indian Institute of Technology Bombay, Mumbai, India AIAA-2004-4411, 10th AIAA/ISSMO Multidisciplinary Analysis and Optimization Conference, Albany, New York, 2004.

[15]Shyy, W., Papila, N., Vaidyanathan, R.,Tucker, K., Global design optimization for aerodynamics and rocket propulsion components, Progress in Aerospace Sciences 37(2001) 59-118.

[16]Palamakula, A., Nutan, M. T. H., and Khan, M. A. "Response Surface Methodology for Optimization and Characterization of Limonene-based Coenzyme Q10 Self-Nanoemulsified Capsule Dosage Form", The AAPS Journal 2004; 6 (3) Article 31.

[17]Myers, R. H., and Montgomery, D. C., "Response Surface Methodology: process and Product optimization using designed experiment", New York: John Wiley and Sons, 1995.

[18]Box, G. E. P., and J. S. Hunter (1957). "Multifactor Experimental Designs for Exploring Response Surfaces." Annals of Mathematical Statistics, Vol. 28,pp. 195-242.

[19]DX, Design-Expert, Software Package, Ver. 6.0.11, Stat-Ease Inc., Minneapolis, MN, 2005.

American Institute of Aeronautics and Astronautics